

# Adversarial Manifold Matching via Deep Metric Learning for Generative Modeling

Mengyu Dai\*  
Microsoft

mendai@microsoft.com

Haibin Hang\*  
University of Delaware

haibin@udel.edu

## Abstract

*We propose a manifold matching approach to generative models which includes a distribution generator (or data generator) and a metric generator. In our framework, we view the real data set as some manifold embedded in a high-dimensional Euclidean space. The distribution generator aims at generating samples that follow some distribution condensed around the real data manifold. It is achieved by matching two sets of points using their geometric shape descriptors, such as centroid and  $p$ -diameter, with learned distance metric; the metric generator utilizes both real data and generated samples to learn a distance metric which is close to some intrinsic geodesic distance on the real data manifold. The produced distance metric is further used for manifold matching. The two networks are learned simultaneously during the training process. We apply the approach on both unsupervised and supervised learning tasks: in unconditional image generation task, the proposed method obtains competitive results compared with existing generative models; in super-resolution task, we incorporate the framework in perception-based models and improve visual qualities by producing samples with more natural textures. Both theoretical analysis and real data experiments guarantee the feasibility and effectiveness of the proposed framework.*

1

## 1. Introduction

Deep generative models including Variational Autoencoder (VAE) [17], Generative Adversarial Networks (GAN) [10] and their variants [3, 21, 20, 33, 8, 32] have achieved great success in generative tasks such as image and video synthesis, super-resolution (SR), image-to-image translation, text generation and so on. The above approaches try to generate samples which mimic real data by minimizing various discrepancies between their corresponding

statistical distributions, such as using KL divergence [17], Jensen-Shannon divergence [10], Wasserstein distance [3], Maximum Mean Discrepancy [21] and others. These approaches focused on the data distribution aspect and did not pay enough attention to the underlying metrics of these distributions. The interplay between distribution measure and its underlying metric is a central topic in optimal transport (cf. [37]). Despite that researchers have successfully employed optimal transport theory in generative models [3, 40, 7], simply assuming the underlying metric to be Euclidean metric may neglect some rich information lying in the data [1]. In addition, although the above approaches are validated to be effective, successful training setups are mostly based on empirical observations with lack of interpretations and physical explanations.

In this paper we bring up a new view for generative modeling – a geometric perspective. Instead of directly matching statistical discrepancies between data distributions, we provide a more robust and flexible framework for modeling data, which is built upon learning distances between data points. The learned distances can not only be used to formulate an energy-based loss function [18] for matching data manifolds, but also describe relations between data points as meaningful interpretations. More specifically, we treat the real data set as some manifold embedded in a high-dimensional Euclidean space, and try to optimize a manifold matching objective to produce a distribution measure condensed around the real data manifold. The manifold matching (MM) objective is built on shape descriptors, such as centroid and  $p$ -diameter, described by proper choice of learned metric. The metric is produced by a metric generator using metric learning approaches. During a training process, the data generator keeps matching the shape descriptors, and the metric generator keeps updating the underlying metric which is further used for manifold matching.

The proposed framework is applied to two tasks: unconditional image generation and single image super-resolution (SISR). We utilize unconditional image generation task as a validation of the feasibility of the approach. We further implement a supervised version of the framework on SISR

<sup>1</sup>\* Equal contributions.

task. SISR aims to recover a high-resolution (HR) image from a low-resolution (LR) one. Soh [36] *et al.* proposed natural manifold discriminator as naturalness loss (or perceptual loss), which tries to distinguish real images from manually generated noisy and blurry ones. The binary classifier serves as a perceptual component in perception-oriented SR models [19, 34, 38, 36]. Since the natural manifold discriminator focuses on classifying certain types of manually generated fake data, one following question is: can we find a more robust way to distinguish real and fake images and learn useful information from real data? Hence we view one usage of our work in SR task as an extension of the natural manifold discriminator, which aims to produce more natural textures from images and mitigate the artifact issue lying in perception-based models.

(1) We propose a manifold matching approach for generative modeling, which tries to match geometric descriptors between real and generated data sets using distances learned during training;

(2) We provide a robust and flexible framework for modeling data and building objectives, where each generator has its own designated objective function;

(3) We conduct experiments on unconditional image generation task which validates the effectiveness of the proposed framework. We further apply the approach on SISR task, which improves both distortion-oriented and perception-based performances on benchmark datasets.

## 2. Related Work

**Manifold Matching:** Shen *et al.* [35] proposed a nonlinear manifold matching algorithm using shortest-path distance and joint neighborhood selection, and illustrated its usage in medical imaging applications. Priebe *et al.* [31] investigated in manifold matching task from the perspective of jointly optimizing the fidelity and commensurability, with an application in document matching. Park *et al.* [30] added a manifold matching loss in GAN objectives which tried to match geometric descriptors using kernel tricks. However, the learning process highly relies on optimizing objectives in the original GAN framework. In addition, without proper metrics, using pre-defined kernels may fail to match the true shapes of data manifolds. In our work, the manifold matching is implemented using geometric descriptors under proper metrics learned by a metric generator.

**Deep Metric Learning:** Among rich sources of literature on deep metric learning, we mainly focus on a few that are related to our work. Xing *et al.* [41] first proposed distance metric learning with applications to improve clustering performance. Hoffer and Ailon implemented deep metric learning with Triplet network [14] which aimed to learn useful representations through distance comparisons. Duan *et al.* [9] proposed a deep adversarial metric learning framework to generate synthetic hard negatives from nega-

tive samples. The hard negative generator and feature embedding were trained simultaneously to learn more precise distance metrics. The metrics were learned in a supervised fashion and then used in classification tasks. Unlike [9], our approach utilizes geometric descriptors for matching data manifolds to generate data without using any labelled information. Mohan *et al.* [29] proposed a direction regularization method which tried to improve the representation space being learnt by guiding the pairs move towards right directions in the metric space. In this work, we utilize the approach in [29] for implementation, while one can use other techniques to approximate distance metrics as well.

**Perception-Based SISR:** Ledig *et al.* [19] first incorporated adversarial component in their objective and achieved high perceptual quality. However, SRGAN can generate observable artifacts such as undesirable noise and whitening effect. Sajjadi *et al.* [34] also utilized GAN adversarial loss and tried to learn realistic textures from high resolution ground truth. The drawback is similar as SRGAN with different types of artifacts. Wang *et al.* [38] proposed ESRGAN which improved perceptual quality by improving SRGAN network architecture and combining PSNR-oriented network and a GAN-based network to balance perceptual quality and fidelity. Soh *et al.* [36] introduced natural manifold discriminator which tried to distinguish real and generated noisy and blurry samples. However, the domain of generated noisy and blurry images is limited and hard to cover real-world sophisticated cases. Ma *et al.* [23] proposed a gradient branch which provides additional structure priors for the SR process. Utilization of the gradient branch need corresponding network architectures to be equipped with. In this paper we propose a method which works towards a different direction regardless of generator architecture, while it can be incorporated into existing methods to potentially improve results.

## 3. Methodology

### 3.1. Proposed Framework

We propose a manifold matching framework for generative modeling which contains a distribution generator  $f_\theta : \mathbb{R}^m \rightarrow \mathbb{R}^D$  and a metric generator  $g_w : \mathbb{R}^D \rightarrow \mathbb{R}^n$ .

$$\mathbb{R}^m \xrightarrow{f_\theta} \mathbb{R}^D \xrightarrow{g_w} \mathbb{R}^n$$

The metric generator  $g_w$  would produce some metric  $d$  on  $\mathbb{R}^D$  to be the pullback of the Euclidean metric  $d_E$  on  $\mathbb{R}^n$  (see Definition 3.2). The distribution generator  $f_\theta$  would produce some measure  $\mu$  on  $\mathbb{R}^D$  to be the pushforward of some prior distribution  $\nu$  on  $\mathbb{R}^m$  (see Definition 3.1). In our implementation,  $m, D, n$  represent dimensions of input variable, target image, and image embedding respectively.

Now we have a metric measure space  $(\mathbb{R}^D, d, \mu)$ . The space of real data is viewed as some manifold  $M \subseteq \mathbb{R}^D$

embedded in Euclidean space. The measure  $\mu$  is said to be condensed around manifold  $M$  if the majority of the measure  $\mu$  distributed nearby  $M$  (see Fig. 1). The manifold  $M$  is called totally geodesic (or “straight”) with respect to metric  $d$  if for any two points  $a, b \in M$ , the shortest path measured by metric  $d$  stays on  $M$  (see Fig. 2). Using the generators  $f_\theta, g_w$  modeled as neural networks, we aim to find proper parameters  $\theta$  and  $w$  such that the induced metric  $d$  and measure  $\mu$  satisfies:

- (1)  $\mu$  is as condensed as possible around  $M$ ;
- (2)  $M$  is as “straight” as possible under  $d$ .

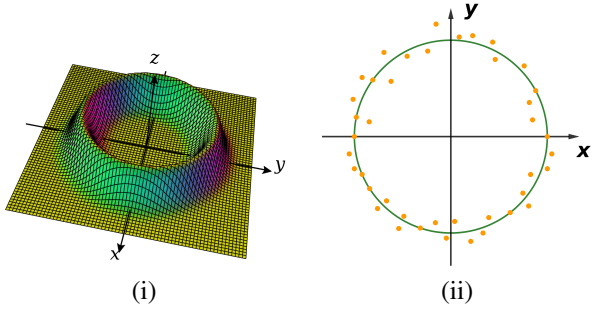


Figure 1. (i) The probability density function of a distribution  $\mu$  which condensed around a circle (manifold)  $M \subseteq \mathbb{R}^2$ ; (ii) The orange dots represents random samples of  $\mu$  and the green circle represents the real data manifold  $M \subseteq \mathbb{R}^2$ .

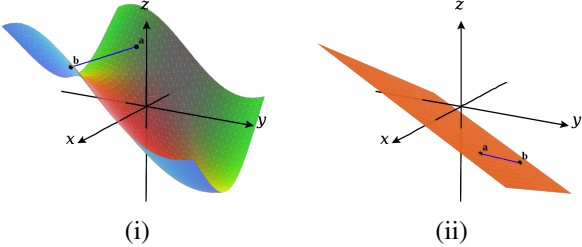


Figure 2. The blue segment represents the shortest path between two points  $a, b$  with respect to Euclidean distance  $d_E$ . (i) A non-geodesic sub-manifold of  $\mathbb{R}^3$  under  $d_E$ ; (ii) A geodesic manifold of  $\mathbb{R}^3$  under  $d_E$ .

Generally speaking, the two networks would produce a sequence of metrics  $\{d_{2i}\}_{i \geq 0}$  and a sequence of measures  $\{\mu_{2i+1}\}_{i \geq 0}$  inductively and alternatively as follows: (i) Let  $d_0 = d_E$ ; Then for any  $i > 0$ , (ii) derive measure  $\mu_{2i-1}$  using manifold matching based on metric  $d_{2i-2}$ ; (iii) derive metric  $d_{2i}$  using metric learning based on measure  $\mu_{2i-1}$ .

$$d_0 = d_E \rightsquigarrow \mu_1 \rightsquigarrow d_2 \rightsquigarrow \mu_3 \rightsquigarrow d_4 \rightsquigarrow \dots$$

In the following we introduce how to implement manifold matching and metric learning in details.

### 3.2. Manifold Matching

Let  $\mathcal{P}(X)$  be the set of all probability measures on space  $X$ . Let  $\mathcal{D}(X)$  be the set of all metrics on space  $X$ . (Proofs

for all properties appeared in this section can be found in supplementary material.)

**Definition 3.1** (Pushforward measure). Given a map  $f : X \rightarrow Y$  and a probability measure  $\mu \in \mathcal{P}(X)$ , the push forward measure  $f_*(\mu) \in \mathcal{P}(Y)$  is defined as: for any measurable set  $A \subseteq Y$ ,

$$(f_*\mu)(A) := \mu(f^{-1}(A)).$$

**Definition 3.2** (Pullback metric). Given a map  $g : Y \rightarrow Z$  and a metric  $d \in \mathcal{D}(Z)$ , the pull back metric  $g^*(d) \in \mathcal{D}(Y)$  is defined as: for any  $y_1, y_2 \in Y$ ,

$$(g^*d)(y_1, y_2) := d(g(y_1), g(y_2)).$$

Manifold matching in our work refers to finding parameter  $\theta_0$  of a specific generative network  $f_\theta : \mathbb{R}^m \rightarrow \mathbb{R}^D$  such that the pushforward  $(f_{\theta_0})_*\nu$  of some prior distribution  $\nu$  via  $f_{\theta_0}$  is condensed around a manifold  $M \subseteq \mathbb{R}^D$ . In our case, the real data manifold  $M \subseteq \mathbb{R}^D$  generally has no explicit expression. In other words, given a point  $a \in \mathbb{R}^D$  these is no way to explicitly tell whether  $a \in M$  or how far away  $a$  is from  $M$ . For this reason, we attempt to estimate the shape of  $M$  via a set of sample points from  $M$ .

The centroid of a space is an important descriptor of its shape. For a metric measure space, the Fréchet mean (cf. [11, 6, 4]) is a natural generalization of the centroid:

**Definition 3.3** (Fréchet mean). The Fréchet mean set  $\sigma(\mathcal{X})$  of a metric measure space  $\mathcal{X} = (X, d, \mu)$  is defined as

$$\arg \min_{x \in X} \int_X d^2(x, y) d\mu(y).$$

Intuitively,  $\sigma(\mathcal{X})$  represents the center of  $\mathcal{X}$  with respect to metric  $d$ . Particularly,

**Lemma 3.4.** *The Fréchet mean of measure  $\mu$  with respect to  $d_E$  coincides with the mean  $\bar{\mu} := \int_{\mathbb{R}^D} y d\mu(y)$ .*

When the underlying metric  $d$  is not the Euclidean metric, the Fréchet mean provides a better option of centroid.

Let  $x_1, x_2, \dots, x_k, \dots$  be a sequence of independent identically distributed points sampled from  $\mu$ . Let  $\mu_k = \frac{1}{k} \sum_{i=1}^k \delta_{x_i}$  denote the empirical measure. We can estimate the Fréchet mean of  $(X, d, \mu)$  by a set of random samples:

**Proposition 3.5.**  $\sigma(\mathcal{X}) = \lim_{k \rightarrow \infty} \sigma(X, d, \mu_k)$ .

The Fréchet mean roughly informs the center of  $\mathcal{X}$ , but to reach the goal of manifold matching, we also need a shape descriptor indicating the size of  $\mathcal{X}$ . Hence we introduce the notion of  $p$ -diameter [26]:

**Definition 3.6** ( $p$ -diameter). For any  $p \geq 1$ , the  $p$ -diameter of metric measure space  $\mathcal{X} := (X, d, \mu)$  is defined as

$$\text{diam}_p(\mathcal{X}) := \left( \int_X \int_X d(x, x')^p d\mu(x) d\mu(x') \right)^{1/p}.$$

The following lemma explains its geometric meaning:

**Lemma 3.7.** For any metric measure space  $\mathcal{X} := (X, d, \mu)$  with  $\text{supp}[\mu] = X$ ,

1.  $\text{diam}_p(\mathcal{X}) \leq \text{diam}_q(\mathcal{X})$  for any  $p \leq q$ ;
2.  $\lim_{p \rightarrow \infty} \text{diam}_p(\mathcal{X}) = \sup_{x, x' \in X} d(x, x')$ .

Similarly, we can estimate the  $p$ -diameter of a metric measure space  $\mathcal{X} := (X, d, \mu)$  by a set of random samples:

**Proposition 3.8.**

$$\text{diam}_p(\mathcal{X}) = \lim_{k \rightarrow \infty} \text{diam}_p(X, d, \mu_k).$$

The above definitions of Fréchet mean and  $p$ -diameter are for metric measure spaces, but it also applies to any manifold assuming a uniform volume measure on it. If we have a set  $S = \{x_1, x_2, \dots, x_k\}$  of sample points from  $\mathcal{X} = (X, d, \mu)$ , then  $(S, d, \mu_k)$  becomes a metric measure space and we simply denote  $\sigma(S) := \sigma(S, d, \mu_k)$  and  $\text{diam}_p(S) := \text{diam}_p(S, d, \mu_k)$ .

When we try to estimate the  $p$ -diameter by a set  $S$  of random samples, if  $p$  is relatively large,  $\text{diam}_p(S)$  is very sensitive to the outliers. To ensure a trustworthy estimation, we choose  $p = 2$  and use  $\text{diam}_2$  as a size indicator.

Let  $S_R$  be a set of random real data samples of  $M$  and  $S_F$  be a set of random fake data samples of  $\mu = (f_\theta)_* \nu$ . Then the objective function we propose for manifold matching is:

$$L_{MM} := d(\sigma(S_R), \sigma(S_F)) + \lambda |\text{diam}_2(S_R) - \text{diam}_2(S_F)|, \quad (1)$$

where  $\lambda$  is a weight parameter.

### 3.3. Metric Learning

In our work shape descriptors in manifold matching greatly rely on a proper choice of metric  $d$ . Even though in the most cases Euclidean metric  $d_E$  is easy to access, it may not be an intrinsic choice and barely reveals the actual shape of a data set.

The intrinsic metric on a Riemannian manifold  $M$  is specified by geodesic distance. Specifically, the geodesic distance between two points on the manifold equals the length of shortest path on  $M$  which connects them. From this point of view, a better choice of metric on the ambient space  $\mathbb{R}^D \supseteq M$  should make the shortest path connecting  $a, b \in M$  stay as close as possible to  $M$ , or in other words, make  $M$  as “straight” as possible.

Here we apply Triplet metric learning to learn a intrinsic metric on  $\mathbb{R}^D$ :

**Definition 3.9.** Given a triple  $(x_a, x_p, x_n)$  with  $x_a, x_p \in M$  and  $x_n \notin M$ , the Triplet loss is defined as

$$L_{tri} := \max\{d^2(x_a, x_p) - d^2(x_a, x_n) + \alpha, 0\},$$

where  $d = (g_w)^* d_E$  and  $\alpha$  is a margin parameter.

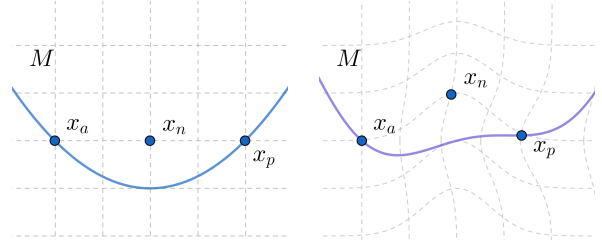


Figure 3. Optimizing the Triplet objective would push out the negative sample  $x_n$  and pull back positive sample  $x_p$ . Intuitively, the learned metric could “distort” the space and “straighten” the manifold.

People usually call  $x_a$  an anchor sample,  $x_p$  a positive sample and  $x_n$  a negative sample. By minimizing  $L_{tri}$ , we attempt to pull back the positive sample to anchor and push out the negative sample, only when  $d(x_a, x_p)$  is relatively larger than  $d(x_a, x_n)$ . Fig. 3 depicts how this would “straighten” the manifold. Note that the Triplet loss may compact the real samples while training, however, in our framework the adversarial learning mechanism always generates fake samples nearby the real data manifold. This behavior guarantees that the triplet loss would not reduce its force to straighten the real data manifold along the training process.

Among numerous methods for metric learning, in our implementation we choose one recent approach [29] which adapted Triplet loss by adding a direction regularizer to make the metric learned towards right direction. Hence in our paper the Triplet loss becomes:

$$L_{apn} = \max\{d^2(x_a, x_p) - d^2(x_a, x_n) + \alpha - \gamma \text{Cos}(g_w(x_n) - g_w(x_a), g_w(x_p) - g_w(x_a)), 0\}. \quad (2)$$

where  $d = (g_w^*) d_E$  and  $\gamma$  is the direction guidance parameter which controls the magnitude of regularization applied to the original loss. In practice one can also employ other methods to learn proper distance metrics.

### 3.4. Objective Functions

In the metric learning community, the metric generator  $g_w$  is usually viewed as a metric embedding. From this point of view we have (see supplement for the proof):

**Proposition 3.10.** Given two measure  $\mu_1$  and  $\mu_2$  on the same metric space  $(X, d)$ , where  $d = g^* d_E$ . Then  $d(\sigma(X, d, \mu_1), \sigma(X, d, \mu_2)) = d_E(\overline{g_* \mu_1}, \overline{g_* \mu_2})$ .

Let  $\|\cdot\|$  denote  $L^2$  norm and  $d = (g_w)^* d_E$ , then we have  $d(x, x') = \|g_w(x) - g_w(x')\|$  for  $\forall x, x' \in \mathbb{R}^D$ . By above proposition, the explicit formula of terms in our objective functions (1) are as follows:

$$d(\sigma(S_R), \sigma(S_F)) = \|\overline{g_w(S_R)} - \overline{g_w(S_F)}\|,$$

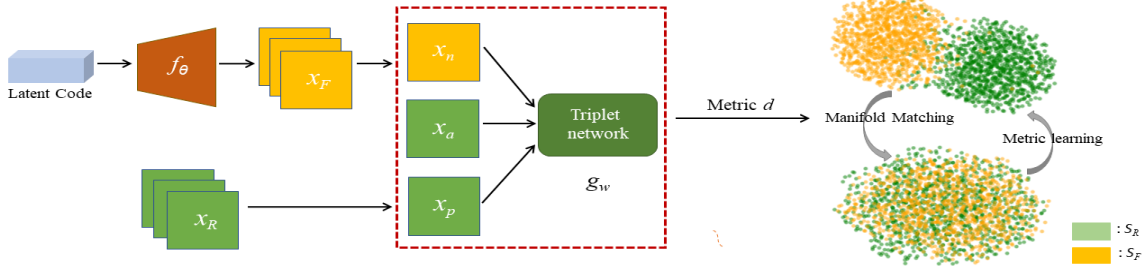


Figure 4. **Implementation pipeline of the proposed framework.**  $x_R$  and  $x_F$  represent samples in real data set  $S_R$  and generated data set  $S_F$  respectively. The distribution (data) generator  $f_\theta$  outputs samples  $x_F \in S_F$  based on manifold matching criteria using learned metric. For Triplet metric learning, anchor samples  $x_a$  and positive samples  $x_p$  are randomly selected from  $S_R$ , and negative samples  $x_n$  are randomly selected from  $S_F$ , without labelled data involved in this step. Learned distance metric is then used for matching data manifolds.

$$\text{diam}_2(S) = \frac{1}{\text{card}(S)} \left( \sum_{x, x' \in x_R} \|g_w(x) - g_w(x')\|^2 \right)^{1/2}.$$

For unconditional image generation task, we take Eqn (1) as manifold matching loss function, and Eqn (2) as metric learning loss. During the training process we try to minimize (1) and (2) simultaneously.

We display our implementation pipeline for unconditional image generation task in Fig 4 and summarize the training procedure in Algorithm 1.

---

**Algorithm 1** Metric learning assisted manifold matching

---

**Input:** Real data manifold  $M$ , prior distribution  $\nu$

**Output:** Distribution generator and metric generator parameters  $\theta, w$

**while**  $\theta$  has not converged **do**

  Sample real data set  $S_R = \{x_1, \dots, x_k\}$  from  $M$ ;

  Sample random noise set  $Z = \{z_1, \dots, z_k\}$  from  $\nu$ ;

$\mathcal{L}_{MM} \leftarrow L_{MM}(S_R, f_\theta(Z))$  in which  $d := (g_w)^* d_E$ ;

$\theta \leftarrow \text{Adam}(\nabla_\theta \mathcal{L}_{MM}, \theta)$

  Sample  $x_a^{(i)}, x_p^{(i)}$  from  $M$  and sample  $z^{(i)}$  from  $\nu, i = 1, 2, \dots, l$ ;

$\mathcal{L}_{apn} \leftarrow \sum_{i=1}^l L_{apn}(x_a^{(i)}, x_p^{(i)}, f_\theta(z^{(i)}))$ ;

$w \leftarrow \text{Adam}(\nabla_w \mathcal{L}_{apn}, w)$ ;

**end while**

---

As for super-resolution task, one can utilize information obtained from LR-HR pairs for more effective matching, thus we include an additional pair matching loss in this case:

$$L_{pair} = \|g_w(x_R^\downarrow) - g_w(x_F^\uparrow)\|,$$

where  $x_F^\uparrow$  is super-resolved image from LR  $x_L$ ,  $x_L^\downarrow$  is down-sampled image from HR  $x_R$  and  $\lambda_2$  is a weight parameter.

We use  $L_1$  loss as pixel-wise image loss, where  $L_{img} = \|x_R^\downarrow - x_F^\uparrow\|_1$ . Together, in SISR task our total data generator loss becomes

$$L_{gen} = L_{img} + \lambda_2 L_{pair} + \lambda_3 L_{MM}. \quad (3)$$

### 3.5. Relation to GAN

The classical GAN is explained as playing a two-player min-max game with a value function, while in our proposed framework, the two networks do not have a common value function. Instead, the two networks compete for distance between real data manifold and generated data distribution. Particularly, one network (distribution generator) tries to produce generated data distribution close to real data manifold with respect a metric  $d$ ; while the other network (metric generator) try to distort metric  $d$  which pushes generated data distribution away from real data manifold. Moreover, discriminators in GANs try to distinguish real and fake samples, or produce their sample statistics. In our framework,  $g_w$  aims at producing metrics for matching geometric descriptors, and can be further used to reveal intrinsic structure of real data manifold. The two networks serve for different purposes under the two frameworks.

From a different point of view, in our framework the two networks also works in a cooperative manner. Each of the two networks has its own designed objective function which build on the information offered by the other network. While exchanging information with each other during training process they both gradually converge. The convergence of training can be addressed using results from [13], (page 3). Particularly, the setting in [13] not only applies to min-max GANs, but is also valid for more general GANs where the discriminator's objective is not necessarily related to the generator's objective. In our framework, using Adam optimizer with different decays for the two networks fits this setting.

## 4. Experiments

We conduct experiments on two tasks: unconditional image generation and single image super-resolution. To better understand the process of manifold matching, in both tasks we track various distances in batches during training. We represent distance between centroids of two sets as  $d_c$ , distance between 2-diameters of two

sets as  $d_g$ , and distance between paired SR-HR samples in super-resolution task as  $d_p$ , respectively. We also use Hausdorff distance as a measurement of distance between the two sets. Hausdorff distance is defined as  $d_H(A, B) = \max \left\{ \sup_{a \in A} \inf_{b \in B} d(a, b), \sup_{b \in B} \inf_{a \in A} d(a, b) \right\}$ , where  $A$  and  $B$  are two non-empty subsets of a metric space  $(\mathcal{M}, d)$ . Here we adopt Euclidean metric to calculate Hausdorff distance between two sets of Triplet network embedding, which is equivalent to measure distance between two sets of corresponding images in the image space. For all experiments we use PyTorch framework for implementation with a Tesla V100 GPU.

### 4.1. Unconditional Image Generation

We use the matching criteria in Eqn 1 to validate the feasibility of the proposed framework. Note that no paired information or GAN loss is used for the task.

**Implementation Details:** We employed a ResNet data generator and a deep convolutional net metric generator with  $\gamma = 0.01$ ,  $\lambda = 1$ , dimension of input latent vector  $z = 128$ , and output embedding  $n = 10$  as our default setting. Adam optimizer with learning rate  $1e - 4$ ,  $\beta_1 = 0$  and  $\beta_2 = 0.9$  for data generator, and  $\beta_1 = 0.5$  and  $\beta_2 = 0.999$  for metric generator was used during training. Details of network architectures are provided in supplementary material.

**Dataset and Evaluation Metrics:** We implemented our method on CelebA [22] and LSUN bedroom [42] datasets. For training we used around 200K images in CelebA and 3M images in LSUN. All images were center-cropped and resized to  $32 \times 32$  or  $64 \times 64$ . For each dataset we randomly generated 50K samples and used Fréchet Inception Distance (FID) [13] for quantitative evaluation. Smaller FID indicates better result.

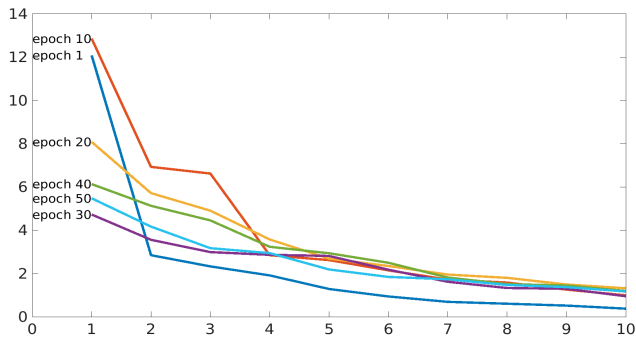


Figure 5. First 10 eigenvalues of distance matrices of 1024 random real data samples during training on CelebA.

**Effect of Metric Learning on Distorting Real Data Manifold:** During training we randomly choose 1024 real samples and detect its shape by looking at the eigenvalues of the corresponding (normalized) distance matrix. Particularly, we plot the first 10 largest eigenvalues which

correspond to the size of the first 10 principle components of real samples. As shown in Figure 5, the shape of the samples becomes more uniform with training going. This is an empirical evidence that  $g_w$  distorts real data manifold to be uniformly curved.

### Effects of Matching Different Geometric Descriptors:

We study the effect of matching different geometric descriptors. Examples of generated  $32 \times 32$  samples on CelebA using different matching criteria are shown in Fig 6. (i) Centroid matching learns some common shallow patterns from real data set; (ii) Matching 2-diameters could capture more complicated inner structures of the data manifold, while misalignment between the two sets can result in low-quality samples (e.g. image on the right side in the second last row); (iii) Combining the two descriptors together leads to more stable sample quality. We also visualize these manifold matching status for illustration purpose. We project Triplet network output embedding to two dimensions by UMAP [25], and display the projected points in Fig 6 (a)(b)(c). (a) and (b) intuitively show two typical matching status if one only matches centroids or 2-diameters between the two sets, respectively.

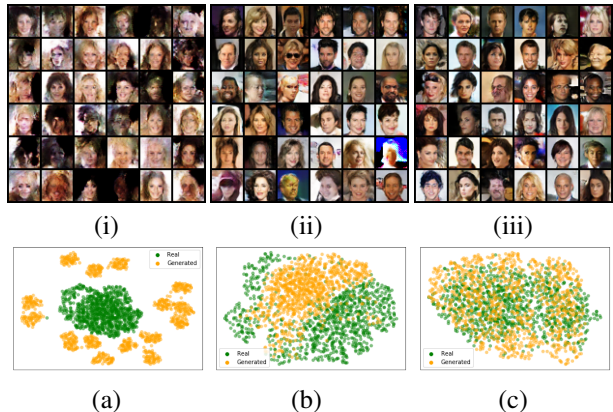


Figure 6. Randomly generated  $32 \times 32$  images on CelebA with different manifold matching criteria during training. (i) centroid only; (ii) 2-diameter only; (iii) both centroid and 2-diameter. (a)(b)(c) are corresponding UMAP plots of real (green) and generated (orange) samples with different manifold matching criteria. (a) centroid only; (b) 2-diameter only; (c) both.

Table 1. Comparisons of results trained on different batch sizes.

Batch size	32	64	128	256	512	1024
Effective training	✓	✓	✓	✓	✓	✗
Time(s) / epoch	178	155	139	127	127	-

**Effects of Batch Size:** We further study the influence of batch size on training time and stability. Table 1 reports average training time per epoch on resized  $32 \times 32$  CelebA images. One can see batch size does not have a significant influence on average training time when matching 2-diameters. In addition, we observe stable and efficient train-

ing sessions with different batch sizes. For batch size as large as 1024, we did not observe satisfying sample quality in reasonable training time.

**Quantitative Results:** We track  $d_c$ ,  $d_g$  and  $d_H$  during training and display them in Fig 7. With training going forward,

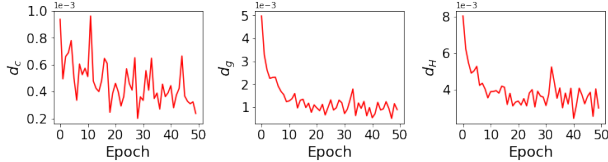


Figure 7. Distances versus training epochs in unconditional image generation task.

the distances keep decreasing and gradually converge. The observation aligns with our manifold matching assumption even with no labelled information involved. For quantitative evaluation we present FID scores in Table 2. Here we also display results from some classic GAN frameworks using the same generator architecture. As shown in the table our method obtains competitive results. Examples of randomly generated samples are displayed in Fig 8. As we see the proposed approach generated visually appealing samples on the two datasets.

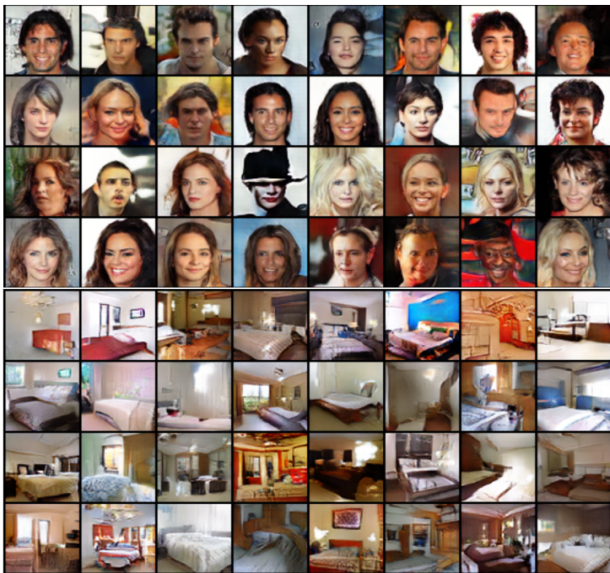


Figure 8. Randomly generated  $64 \times 64$  samples on CelebA and LSUN bedroom.

Table 2. FID evaluation on  $64 \times 64$  experiments with a ResNet generator.

Method	CelebA	LSUN bedroom
WGAN [3]	37.1 (1.9)	73.3 (2.5)
WGAN-GP [12]	18.0 (0.7)	26.9 (1.1)
SNGAN [28]	21.7 (1.5)	31.3 (2.1)
SWGAN [40]	13.2 (0.7)	14.9 (1.0)
Ours	<b>11.1 (0.1)</b>	<b>13.7 (0.3)</b>

## 4.2. Single Image Super-Resolution

In a typical perception-based SR model [19, 36], the generator loss function is usually made up by three components: pixel-wise image loss, GAN loss and perceptual loss (or naturalness loss in [36]). Here we explore the use of our work with two different settings: (A) Our approach (MM) serves as a substitute of GAN loss. In this case we use Eqn 3 as the total generator loss function without involving GAN loss; (B) MM serves as a substitute of naturalness loss. In (B) MM is used as a complement of GAN in perception-based models, where a GAN loss is added to Eqn 3 as the total generator loss.

**Implementation Details:** For setting (A), we compare MM and GAN using three different generator backbones: ResNet [19], RDN [45] and NSRNet [36]. All experiments were conducted with the same training setup. For setting (B), we compare the effects of different perceptual components in perception-based models. We employed the ResNet architecture in [19] as the default generator backbone, and RaGAN [16] with weight  $2e - 3$  as GAN component for consistency. For both (A) and (B) we experimented on  $\times 4$  SR task. We utilized Adam optimizer with learning rate  $1e - 4$ ,  $\beta_1 = 0.9$ ,  $\beta_2 = 0.999$ , metric learning direction guidance parameter  $\gamma = 1e - 2$ , weight of diameter matching term  $\lambda = 1$ , dimension of Triplet network output embedding  $n = 32$ , batch size = 32,  $\lambda_2 = \lambda_3 = 1e - 3$ , and trained for 100K iterations. Details of Triplet network architecture is presented in supplementary material.

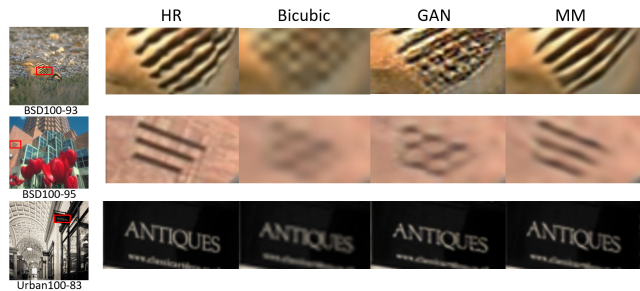


Figure 9. Generated  $\times 4$  samples with GAN loss and MM loss using the same generator backbone. (Zoom in for better view.)

**Datasets and Evaluation Metrics:** We used 800 HR images in DIV2K [2] dataset as training set, and four benchmark datasets: Set5 [5], Set14 [43], BSD100 [24] and Urban100 [15] for testing. HR images were downsampled by bicubic interpolation to get  $48 \times 48$  LR input patches. We evaluated results using Structure Similarity (SSIM) [39], PSNR as distortion-oriented evaluation metrics, and Naturalness Image Quality Evaluator (NIQE) [27], Learned Perceptual Image Patch Similarity (LPIPS) [44] as perception-oriented evaluation metrics. Lower NIQE and LPIPS scores indicate higher perceptual quality.

**Results:** We record  $d_p$ ,  $d_c$ ,  $d_g$ , and Hausdorff distance  $d_H$  during training and display them in Fig.10. One can see

Table 3. Evaluation scores of different training settings in  $\times 4$  SISR task. Demonstration of settings is displayed in Table 4. For each pair of settings with the same generator backbone, the one with better performance is highlighted.

	Set5				Set14				BSD100				Urban100			
Setting	PSNR	SSIM	LPIPS	NIQE												
ResNet-GAN	29.03	0.8468	<b>0.1885</b>	7.2143	25.64	0.7420	0.2761	<b>5.2654</b>	25.74	0.7026	<b>0.3160</b>	<b>5.3896</b>	23.49	0.7273	0.2888	<b>4.6504</b>
ResNet-MM	<b>29.76</b>	<b>0.8606</b>	0.1941	<b>6.1478</b>	<b>26.12</b>	<b>0.7562</b>	<b>0.2724</b>	5.3458	<b>26.07</b>	<b>0.7150</b>	0.3178	5.5508	<b>24.06</b>	<b>0.7505</b>	<b>0.2774</b>	4.7549
RDN-GAN	29.07	0.8442	<b>0.1841</b>	6.6459	25.38	0.7355	0.2729	5.3887	25.72	0.7029	<b>0.3063</b>	5.6734	23.11	0.7190	0.2876	4.6546
RDN-MM	<b>30.06</b>	<b>0.8658</b>	0.1850	<b>6.1283</b>	<b>26.31</b>	<b>0.7615</b>	<b>0.2641</b>	<b>5.2161</b>	<b>26.24</b>	<b>0.7210</b>	0.3100	<b>5.4127</b>	<b>24.44</b>	<b>0.7645</b>	<b>0.2566</b>	<b>4.5914</b>
NSRNet-GAN	29.46	0.8544	0.1852	<b>5.7818</b>	25.93	0.7478	0.2666	<b>5.1213</b>	25.93	0.7094	0.3119	<b>5.2069</b>	23.70	0.7330	0.2832	5.1579
NSRNet-MM	<b>29.79</b>	<b>0.8641</b>	<b>0.1845</b>	6.0846	<b>26.17</b>	<b>0.7590</b>	<b>0.2655</b>	5.3175	<b>26.13</b>	<b>0.7188</b>	<b>0.3114</b>	5.3794	<b>24.19</b>	<b>0.7569</b>	<b>0.2621</b>	<b>4.5937</b>

Table 4. Training settings for GAN-based SISR methods with fixed generator architecture and GAN component.

Setting	Method	Perceptual component	Pretrained
A	Bicubic	-	-
B	GAN-ResNet	-	-
C	SRGAN	VGG16-Pooling5	Yes
D	EnhanceNet	VGG19-Pooling2,5	Yes
E	ESRGAN	VGG19-Conv5-4	Yes
F	NatSR	NMD	Yes
G(ours)	MM	MM	No

all distances keeps decreasing with training going forward, which is aligned with our basic assumption that the two sets of points keep getting close to each other. Note that the spike effect is common for Adam optimizer when feeding some abnormal random batch of training data.

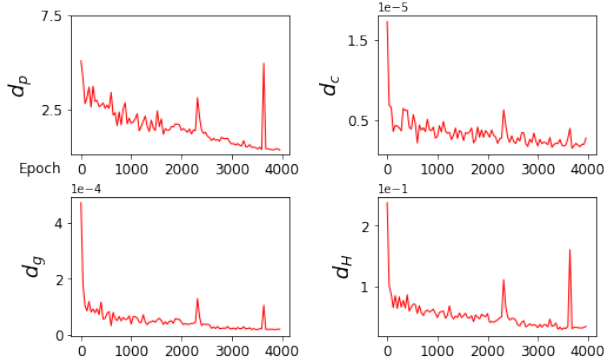


Figure 10. Various distances versus training epochs in super-resolution experiment with our method. Distances are displayed every 40 epochs (1000 iterations).

**(A) MM As A Substitute of GAN Loss:** We display comparison of evaluation results between GAN and MM in Table 3. Under different backbones, MM performs better than GAN in similarity-based metrics in all cases. It also obtains better scores in perception-based metrics in majority of the cases. Examples of generated samples using the same generator backbone are displayed in Fig 9. We see MM resulted in samples with more natural textures.

**(B) MM As A Substitute of Naturalness Loss:** We display a few different setups in Table 4. Final results with both

distortion-based and perception-based evaluation scores on benchmark datasets are presented in Table 5, where GAN-ResNet represents SRGAN without VGG component in loss function. With the same common setup, our method obtained better results in most of the cases for both types of metrics. Examples of generated samples from various settings are shown in Fig 11. As we see the proposed method generates samples with more natural textures and less artifacts under the same setup.

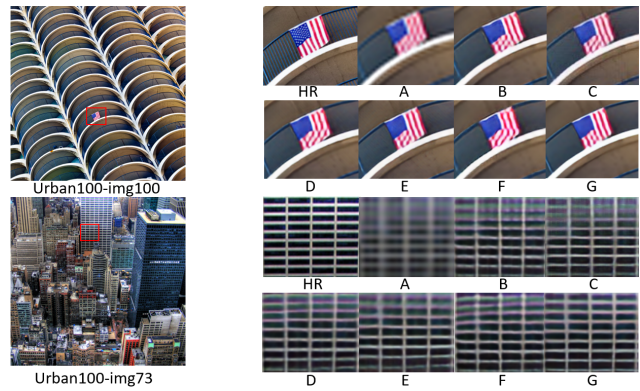


Figure 11. Comparison of generated samples from different settings. All settings were trained with the same ResNet generator backbone and GAN components. (Zoom in for better view.)

Note that although both GAN and MM utilize adversarial learning for training, we notice the two approaches function differently in super-resolution task. GAN tends to generate more details but with artifacts, while MM tends to generate more natural textures in images. The two approaches do not conflict with each other. Instead, one serves as a complement for the other to result in better sample quality.

## 5. Discussion and Conclusion

In this paper, we have proposed a manifold matching approach for generative modeling, which tries to match the geometric descriptors of real and generated data sets using learned distance metrics. Theoretical analysis and real data experiments on two tasks show its feasibility and effectiveness. In addition, the proposed framework is robust and

Table 5. Evaluation scores of different training settings in  $\times 4$  SISR task. Demonstration of settings is displayed in Table 4. The best performance is highlighted in red and second best in blue.

	Set5				Set14				BSD100				Urban100			
Setting	PSNR	SSIM	LPIPS	NIQE	PSNR	SSIM	LPIPS	NIQE	PSNR	SSIM	LPIPS	NIQE	PSNR	SSIM	LPIPS	NIQE
A	28.42	0.8104	0.2977	7.3647	26.00	0.7027	0.3757	6.3393	25.96	0.6675	0.4637	6.2967	23.14	0.6577	0.4182	6.6429
B	29.66	0.8586	0.1401	6.6582	26.08	0.7542	0.2265	5.3638	26.05	0.7145	0.3257	5.5376	24.00	0.7464	0.2156	4.7883
C	29.30	0.8445	0.1324	6.6590	25.81	0.7394	0.2132	5.5318	25.81	0.7010	0.3006	5.8399	23.83	0.7346	0.2047	4.6377
D	29.75	0.8593	0.1357	6.5475	26.11	0.7542	0.2193	5.3559	26.06	0.7145	0.3160	5.6108	24.15	0.7506	0.2028	4.7447
E	29.63	0.8547	0.1227	6.2838	26.07	0.7512	0.2051	5.0657	26.05	0.7119	0.2957	5.2257	24.12	0.7484	0.1862	4.2814
F	29.70	0.8603	0.1409	6.2673	26.06	0.7556	0.2239	5.3777	26.05	0.7146	0.3218	5.6095	23.98	0.7477	0.2126	4.7880
G	29.87	0.8615	0.1281	5.8904	26.17	0.7564	0.2048	4.9612	26.10	0.7134	0.2930	4.9864	24.25	0.7567	0.1866	4.3432

flexible in that each module has its own designated objective. Despite that our method has led to some promising results, there is yet much room for improvements. For example, the currently used geometric descriptors may not fully recover the information of the underlying manifolds, thus matching towards other descriptors could potentially benefit the learning process. As to metric learning, in our paper we employ the framework in [29] fed with random samples to learn a metric for usage, while in practice one could investigate ways for better approximation of metrics, such as utilizing sampling methods or other metric learning methods. In the last few years we have seen the successful evolution of probability-based generative modeling approaches, and we believe joining geometry with statistics would lead to stronger expression ability for generative models, which is a promising direction for researchers to explore. For the theoretical side, the current metric measure space setting may benefit the of use more advanced tools from optimal transport in deep generative models.

## References

- [1] Charu C. Aggarwal, Alexander Hinneburg, and Daniel A. Keim. On the surprising behavior of distance metrics in high dimensional spaces. In *Proceedings of the 8th International Conference on Database Theory*. Springer-Verlag, 2001. 1
- [2] Eirikur Agustsson and Radu Timofte. Ntire 2017 challenge on single image super-resolution: Dataset and study. In *The IEEE Conference on Computer Vision and Pattern Recognition (CVPR) Workshops*, July 2017. 7
- [3] Martin Arjovsky, Soumith Chintala, and Léon Bottou. Wasserstein generative adversarial networks. In *Proceedings of the 34th International Conference on Machine Learning*, volume 70, pages 214–223, 2017. 1, 7
- [4] Marc Arnaudon, Frédéric Barbaresco, and Le Yang. Medians and means in riemannian geometry: existence, uniqueness and computation. In *Matrix Information Geometry*, pages 169–197. Springer, 2013. 3
- [5] Marco Bevilacqua, Aline Roumy, Christine Guillemot, and Marie line Alberi Morel. Low-complexity single-image super-resolution based on nonnegative neighbor embedding. In *Proceedings of the British Machine Vision Conference*, pages 135.1–135.10. BMVA Press, 2012. 7
- [6] Rabi Bhattacharya and Vic Patrangenaru. Large sample theory of intrinsic and extrinsic sample means on manifolds. *The Annals of Statistics*, 31(1):1–29, 2003. 3
- [7] Ishan Deshpande, Yuan-Ting Hu, Ruoyu Sun, Ayis Pyrros, Nasir Siddiqui, Sanmi Koyejo, Zhizhen Zhao, David Forsyth, and Alexander G. Schwing. Max-sliced wasserstein distance and its use for gans. In *Proceedings of the IEEE/CVF Conference on Computer Vision and Pattern Recognition (CVPR)*, June 2019. 1
- [8] Zheng Ding, Yifan Xu, Weijian Xu, Gaurav Parmar, Yang Yang, Max Welling, and Zhuowen Tu. Guided variational autoencoder for disentanglement learning. In *Proceedings of the IEEE/CVF Conference on Computer Vision and Pattern Recognition (CVPR)*, June 2020. 1
- [9] Yueqi Duan, Wenzhao Zheng, Xudong Lin, Jiwen Lu, and Jie Zhou. Deep adversarial metric learning. In *Proceedings of the IEEE Conference on Computer Vision and Pattern Recognition (CVPR)*, June 2018. 2
- [10] Ian Goodfellow, Jean Pouget-Abadie, Mehdi Mirza, Bing Xu, David Warde-Farley, Sherjil Ozair, Aaron Courville, and Yoshua Bengio. Generative adversarial nets. In *Advances in neural information processing systems*, pages 2672–2680, 2014. 1
- [11] Karsten Grove and Hermann Karcher. How to conjugate  $C^1$ -close group actions. *Mathematische Zeitschrift*, 132(1):11–20, 1973. 3
- [12] Ishaan Gulrajani, Faruk Ahmed, Martin Arjovsky, Vincent Dumoulin, and Aaron C Courville. Improved training of wasserstein gans. In I. Guyon, U. V. Luxburg, S. Bengio, H. Wallach, R. Fergus, S. Vishwanathan, and R. Garnett, editors, *Advances in Neural Information Processing Systems*, volume 30, 2017. 7
- [13] Martin Heusel, Hubert Ramsauer, Thomas Unterthiner, Bernhard Nessler, and Sepp Hochreiter. Gans trained by a two time-scale update rule converge to a local nash equilibrium. In *Advances in neural information processing systems*, pages 6626–6637, 2017. 5, 6
- [14] Elad Hoffer and Nir Ailon. Deep metric learning using triplet network. In *International Workshop on Similarity-Based Pattern Recognition*, pages 84–92. Springer, 2015. 2
- [15] Jia-Bin Huang, Abhishek Singh, and Narendra Ahuja. Single image super-resolution from transformed self-exemplars. In *Proceedings of the IEEE Conference on Computer Vision and Pattern Recognition (CVPR)*, June 2015. 7
- [16] Alexia Jolicoeur-Martineau. The relativistic discriminator: a key element missing from standard GAN. *CoRR*, abs/1807.00734, 2018. 7
- [17] Diederik P. Kingma and Max Welling. Auto-Encoding Variational Bayes. In *2nd International Conference on Learning Representations, ICLR 2014, Banff, AB, Canada, April 14-16, 2014, Conference Track Proceedings*, 2014. 1
- [18] Yann LeCun, Sumit Chopra, Raia Hadsell, Fu Jie Huang, and et al. A tutorial on energy-based learning. In *PREDICTING STRUCTURED DATA*. MIT Press, 2006. 1
- [19] Christian Ledig, Lucas Theis, Ferenc Huszár, Jose Caballero, Andrew Cunningham, Alejandro Acosta, Andrew Aitken, Alykhan Tejani, Johannes Totz, Zehan Wang, et al. Photo-realistic single image super-resolution using a generative adversarial network. In *Proceedings of the IEEE conference on computer vision and pattern recognition*, pages 4681–4690, 2017. 2, 7
- [20] Chen-Yu Lee, Tanmay Batra, Mohammad Haris Baig, and Daniel Ulbricht. Sliced wasserstein discrepancy for unsupervised domain adaptation. In *Proceedings of the IEEE/CVF Conference on Computer Vision and Pattern Recognition (CVPR)*, June 2019. 1
- [21] Chun-Liang Li, Wei-Cheng Chang, Yu Cheng, Yiming Yang, and Barnabás Póczos. Mmd gan: Towards

- deeper understanding of moment matching network. In *Advances in Neural Information Processing Systems*, pages 2203–2213, 2017. 1
- [22] Ziwei Liu, Ping Luo, Xiaogang Wang, and Xiaoou Tang. Deep learning face attributes in the wild. In *Proceedings of International Conference on Computer Vision (ICCV)*, December 2015. 6
- [23] Cheng Ma, Yongming Rao, Yean Cheng, Ce Chen, Jiwen Lu, and Jie Zhou. Structure-preserving super resolution with gradient guidance. In *IEEE/CVF Conference on Computer Vision and Pattern Recognition (CVPR)*, June 2020. 2
- [24] David Martin, Charless Fowlkes, Doron Tal, and Jitendra Malik. A database of human segmented natural images and its application to evaluating segmentation algorithms and measuring ecological statistics. In *Proceedings Eighth IEEE International Conference on Computer Vision. ICCV 2001*, volume 2, pages 416–423. IEEE, 2001. 7
- [25] Leland McInnes, John Healy, Nathaniel Saul, and Lukas Großberger. Umap: Uniform manifold approximation and projection. *Journal of Open Source Software*, 3(29):861, 2018. 6
- [26] Facundo Mémoli. Gromov–wasserstein distances and the metric approach to object matching. *Foundations of computational mathematics*, 11(4):417–487, 2011. 3
- [27] Anish Mittal, Rajiv Soundararajan, and Alan C Bovik. Making a “completely blind” image quality analyzer. *IEEE Signal processing letters*, 20(3):209–212, 2012. 7
- [28] Takeru Miyato, Toshiki Kataoka, Masanori Koyama, and Yuichi Yoshida. Spectral normalization for generative adversarial networks. In *International Conference on Learning Representations*, 2018. 7
- [29] Deen Dayal Mohan, Nishant Sankaran, Dennis Fedorishin, Srirangaraj Setlur, and Venu Govindaraju. Moving in the right direction: A regularization for deep metric learning. In *Proceedings of the IEEE/CVF Conference on Computer Vision and Pattern Recognition (CVPR)*, June 2020. 2, 4, 9
- [30] Noseong Park, Ankesh Anand, Joel Ruben Antony Moniz, Kookjin Lee, Jaegul Choo, David Keetae Park, Tanmoy Chakraborty, Hongkyu Park, and Youngmin Kim. Mmgan: Manifold-matching generative adversarial networks. In *2018 24th International Conference on Pattern Recognition (ICPR)*, pages 1343–1348. IEEE, 2018. 2
- [31] Carey E. Priebe, David J. Marchette, Zhiliang Ma Jhu, and Sancar Adali Jhu. Manifold matching: Joint optimization of fidelity and commensurability, 2010. 2
- [32] Kanishka Rao, Chris Harris, Alex Irpan, Sergey Levine, Julian Ibarz, and Mohi Khansari. RL-cyclegan: Reinforcement learning aware simulation-to-real. In *Proceedings of the IEEE/CVF Conference on Computer Vision and Pattern Recognition (CVPR)*, June 2020. 1
- [33] Michal Rolinek, Dominik Zietlow, and Georg Martius. Variational autoencoders pursue pca directions (by accident). In *Proceedings of the IEEE/CVF Conference on Computer Vision and Pattern Recognition (CVPR)*, June 2019. 1
- [34] Mehdi SM Sajjadi, Bernhard Scholkopf, and Michael Hirsch. Enhancenet: Single image super-resolution through automated texture synthesis. In *Proceedings of the IEEE International Conference on Computer Vision*, pages 4491–4500, 2017. 2
- [35] Cencheng Shen, J. Vogelstein, and C. Priebe. Manifold matching using shortest-path distance and joint neighborhood selection. *Pattern Recognit. Lett.*, 92:41–48, 2017. 2
- [36] Jae Woong Soh, Gu Yong Park, Junho Jo, and Nam Ik Cho. Natural and realistic single image super-resolution with explicit natural manifold discrimination. In *The IEEE Conference on Computer Vision and Pattern Recognition (CVPR)*, June 2019. 2, 7
- [37] Cédric Villani. *Optimal transport: old and new*, volume 338. Springer Science & Business Media, 2008. 1
- [38] Xintao Wang, Ke Yu, Shixiang Wu, Jinjin Gu, Yihao Liu, Chao Dong, Yu Qiao, and Chen Change Loy. Esrgan: Enhanced super-resolution generative adversarial networks. In *The European Conference on Computer Vision Workshops (ECCVW)*, September 2018. 2
- [39] Zhou Wang, Alan C. Bovik, Hamid R. Sheikh, and Eero P. Simoncelli. Image quality assessment: From error visibility to structural similarity. *IEEE TRANSACTIONS ON IMAGE PROCESSING*, 13(4):600–612, 2004. 7
- [40] Jiqing Wu, Zhiwu Huang, Dinesh Acharya, Wen Li, Janine Thoma, Danda Pani Paudel, and Luc Van Gool. Sliced wasserstein generative models. In *Proceedings of the IEEE/CVF Conference on Computer Vision and Pattern Recognition (CVPR)*, June 2019. 1, 7
- [41] Eric P Xing, Michael I Jordan, Stuart J Russell, and Andrew Y Ng. Distance metric learning with application to clustering with side-information. In *Advances in neural information processing systems*, pages 521–528, 2003. 2
- [42] Fisher Yu, Yinda Zhang, Shuran Song, Ari Seff, and Jianxiong Xiao. Lsun: Construction of a large-scale

image dataset using deep learning with humans in the loop. *CoRR*, abs/1506.03365, 2015. 6

- [43] Roman Zeyde, Michael Elad, and Matan Protter. On single image scale-up using sparse-representations,” curves and surfaces, 2012. 7
- [44] Richard Zhang, Phillip Isola, Alexei A Efros, Eli Shechtman, and Oliver Wang. The unreasonable effectiveness of deep features as a perceptual metric. In *Proceedings of the IEEE conference on computer vision and pattern recognition*, pages 586–595, 2018. 7
- [45] Yulun Zhang, Yapeng Tian, Yu Kong, Bineng Zhong, and Yun Fu. Residual dense network for image super-resolution. In *Proceedings of the IEEE conference on computer vision and pattern recognition*, pages 2472–2481, 2018. 7

## 6. Appendix: Proofs of Properties

Given any space  $X$  associated with a probability measure  $\mu$  s.t.  $\text{supp}[\mu] = X$  and  $p \geq 1$ , then for any function  $f : X \rightarrow \mathbb{R}$  we denote its  $L^p$  norm as

$$\|f\|_p := \left( \int_X |f(x)|^p d\mu(x) \right)^{1/p}.$$

Then we have the following properties:

**Lemma 6.1.** Denote  $\|f\|_\infty := \sup_{x \in X} f(x)$ , then

1. If  $p \leq q$ , then  $\|f\|_p \leq \|f\|_q$ ;
2.  $\lim_{p \rightarrow \infty} \|f\|_p = \|f\|_\infty$ .

*Proof.* Let  $r = q/p$  and  $s$  be such that  $1/r + 1/s = 1$ . Let  $a(x) = |f(x)|^p$  and  $b(x) \equiv 1$ , then by Holder's inequality, we have

$$\|ab\|_1 \leq \|a\|_r \|b\|_s$$

or

$$\int_{x \in X} |f(x)|^p d\mu(x) \leq \left( \int_{x \in X} |f(x)|^{p \cdot \frac{q}{p}} d\mu(x) \right)^{p/q}.$$

Now taking the  $p$ -th root on both sides we obtain  $\|f\|_p \leq \|f\|_q$ .

It is easy to see  $\|f\|_p \leq \|f\|_\infty$  for any  $p > 1$ . Now we choose  $\forall \epsilon > 0$  with  $\epsilon < \|f\|_\infty$  and let  $X_\epsilon := \{x \in X \mid f(x) \geq \|f\|_\infty - \epsilon\}$ , then

$$\begin{aligned} & \left( \int_{x \in X} |f(x)|^p d\mu(x) \right)^{1/p} \\ & \geq \left( \int_{X_\epsilon} (\|f\|_\infty - \epsilon)^p d\mu(x) \right)^{1/p} \\ & = (\|f\|_\infty - \epsilon) \mu(X_\epsilon)^{1/p} \end{aligned}$$

When  $p \rightarrow \infty$  we have  $\lim_{p \rightarrow \infty} \|f\|_p \geq \|f\|_\infty - \epsilon$ . Since  $\epsilon$  is arbitrary we have  $\lim_{p \rightarrow \infty} \|f\|_p \geq \|f\|_\infty$ .  $\square$

*Proof of Lemma 3.4.* Suppose that elements in  $\mathbb{R}^D$  are represented as column vectors. Then  $\sigma(\mathbb{R}^D, d, \mu)$  equals the set of minimizers of

$$F(x) = \int_{\mathbb{R}^D} (y-x)^T (y-x) d\mu(y).$$

Since  $\frac{\partial F}{\partial x} = -2 \int_{\mathbb{R}^D} y d\mu(y) + 2x$ , let  $\frac{\partial F}{\partial x} = 0$  we have single minimizer of  $F(x)$  to be  $\int_{\mathbb{R}^D} y d\mu(y) = \bar{\mu}$ .  $\square$

*Proof of Proposition 3.5.* Since the empirical measure  $\mu_k$  weakly converges to  $\mu$ , the result following by the definition of weak convergence.  $\square$

*Proof of Lemma 3.7.* It follows directly from Lemma 6.1  $\square$

*Proof of Proposition 3.8.* Since the empirical measure  $\mu_k$  weakly converges to  $\mu$ , the result following by the definition of weak convergence.  $\square$

**Proposition 6.2.** Given a metric measure space  $\mathcal{X} := (X, d, \mu)$  and map  $g : X \rightarrow \mathbb{R}^n$ . If  $d = g^* d_E$ , then

$$\sigma(\mathcal{X}) = g^{-1}(\overline{g_* \mu}).$$

*Proof.* By definition,  $\sigma(\mathcal{X})$  is the set of minimizers of function

$$\begin{aligned} F(x) &:= \int_X (g^* d_E)^2(x, y) d\mu(y) \\ &= \int_X d_E^2(g(x), g(y)) d\mu(y) \\ &= \int_{\mathbb{R}^n} d_E^2(g(x), z) d(g_* \mu)(z). \end{aligned}$$

It is easy to see that  $x_0$  is a minimizer of  $F(x)$  iff.  $g(x_0)$  is a minimizer of  $G(w) := \int_{\mathbb{R}^n} d_E^2(w, z) d(g_* \mu)(z)$ . By Lemma 3.4,  $\overline{g_* \mu} = \text{argmin } G(w)$ , hence we have  $\sigma(\mathcal{X}) = \text{argmin } F(x) = g^{-1}(\overline{g_* \mu})$ .  $\square$

*Proof of Proposition 3.10.* It follows directly from Proposition 6.2  $\square$